Cell Reports, Volume *35*

Supplemental information

Anterior insula regulates brain network transitions that gate conscious access

Zirui Huang, Vijay Tarnal, Phillip E. Vlisides, Ellen L. Janke, Amy M. McKinney, Paul Picton, George A. Mashour, and Anthony G. Hudetz

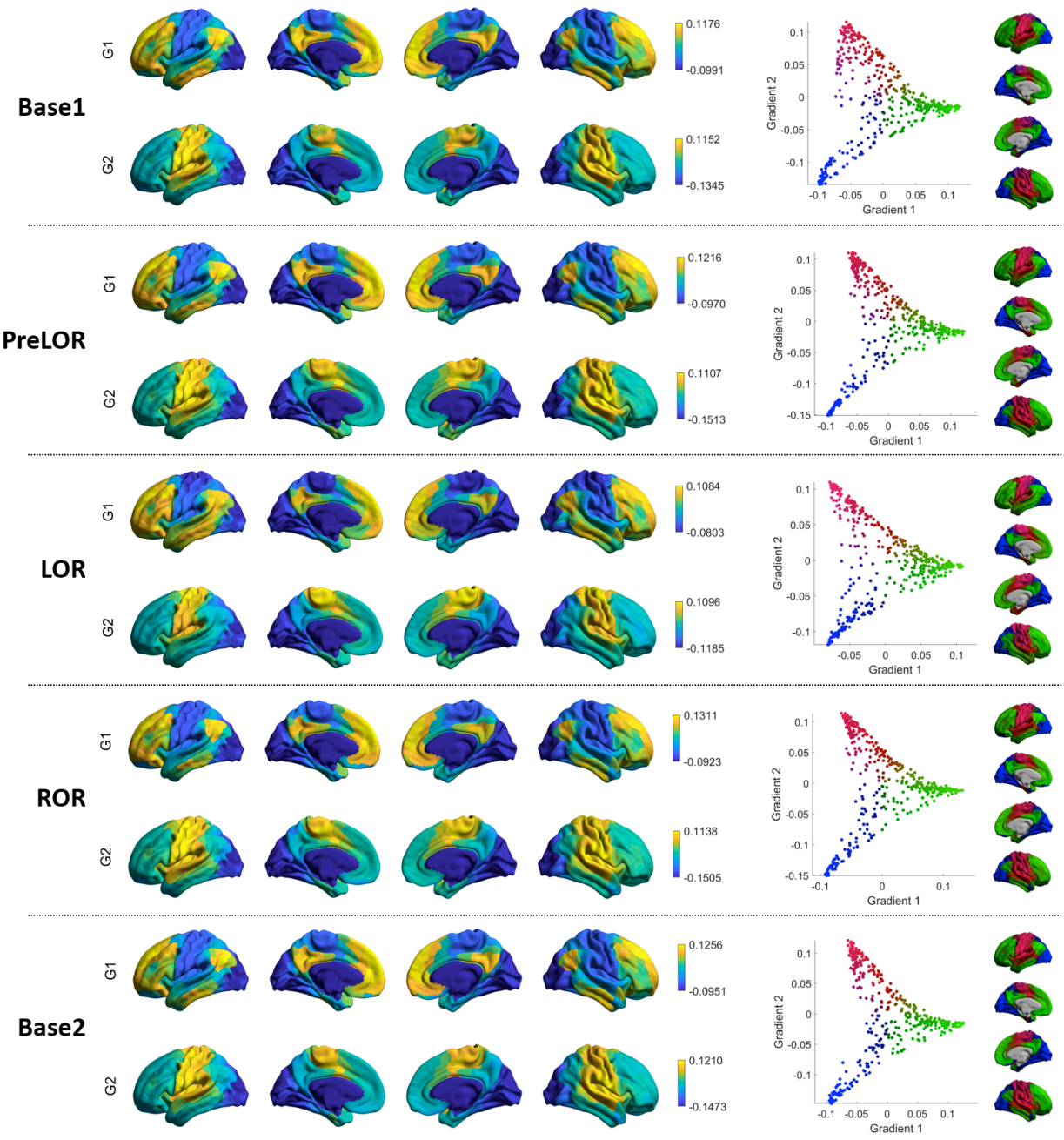

Figure S1. Cortical gradients across different conditions. Related to Figure 3. Left panel: topographic profiles of the first two gradients along the cortex. Right penal: the two gradients are projected into a 2-dimensional gradient space. The axes of the 2-dimensional space represent each gradient and separate distinct functional poles of cortical organization.

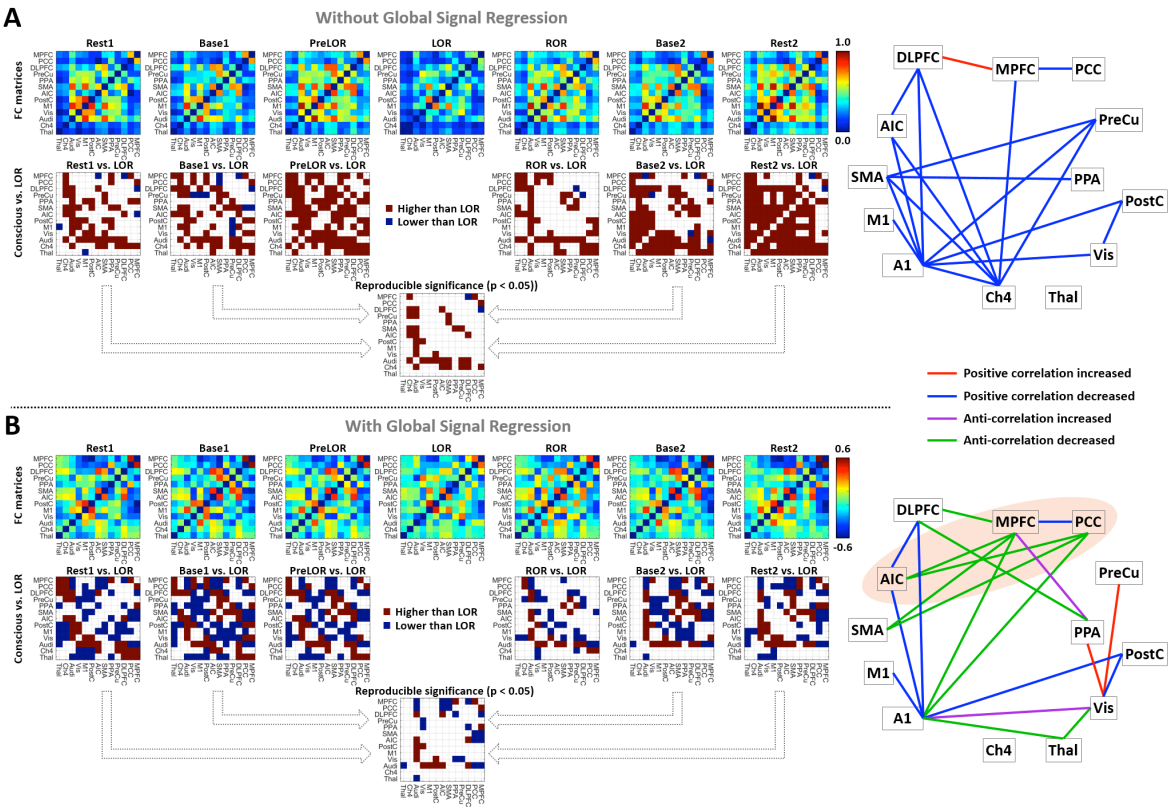

Figure S2. Functional connectivity among brain regions. Related to Figure 6. **(A)** Results without applying global signal regression (non-GSR). **(B)** Results after global signal regression (GSR). The time courses of fMRI signal change were extracted from the pre-defined ROIs for each condition, including Rest1 (n=26), Base1 (n=26), PreLOR (n=26), LOR (n=26), ROR (n=16), Base2 (n=25), and Rest2 (n=25). Qualitative estimation of functional connectivity was performed by calculating Pearson's correlation coefficient (Fisher's Z transformed) for each pair of ROIs. Individual pairwise functional connectivity matrices were generated for each condition. The reproducible differences across Rest1 vs. LOR, Base1 vs. LOR, Base2 vs. LOR, and Rest2 vs. LOR (two-sample paired sample t-tests; statistical significance at $p<0.05$) were considered as the genuine functional connectivity alterations during LOR (see connectivity matrix in lower, center position), with potential spurious functional connectivity driven by task-evoked activity accounted for. Schematics on the right summarize the effects of interest.

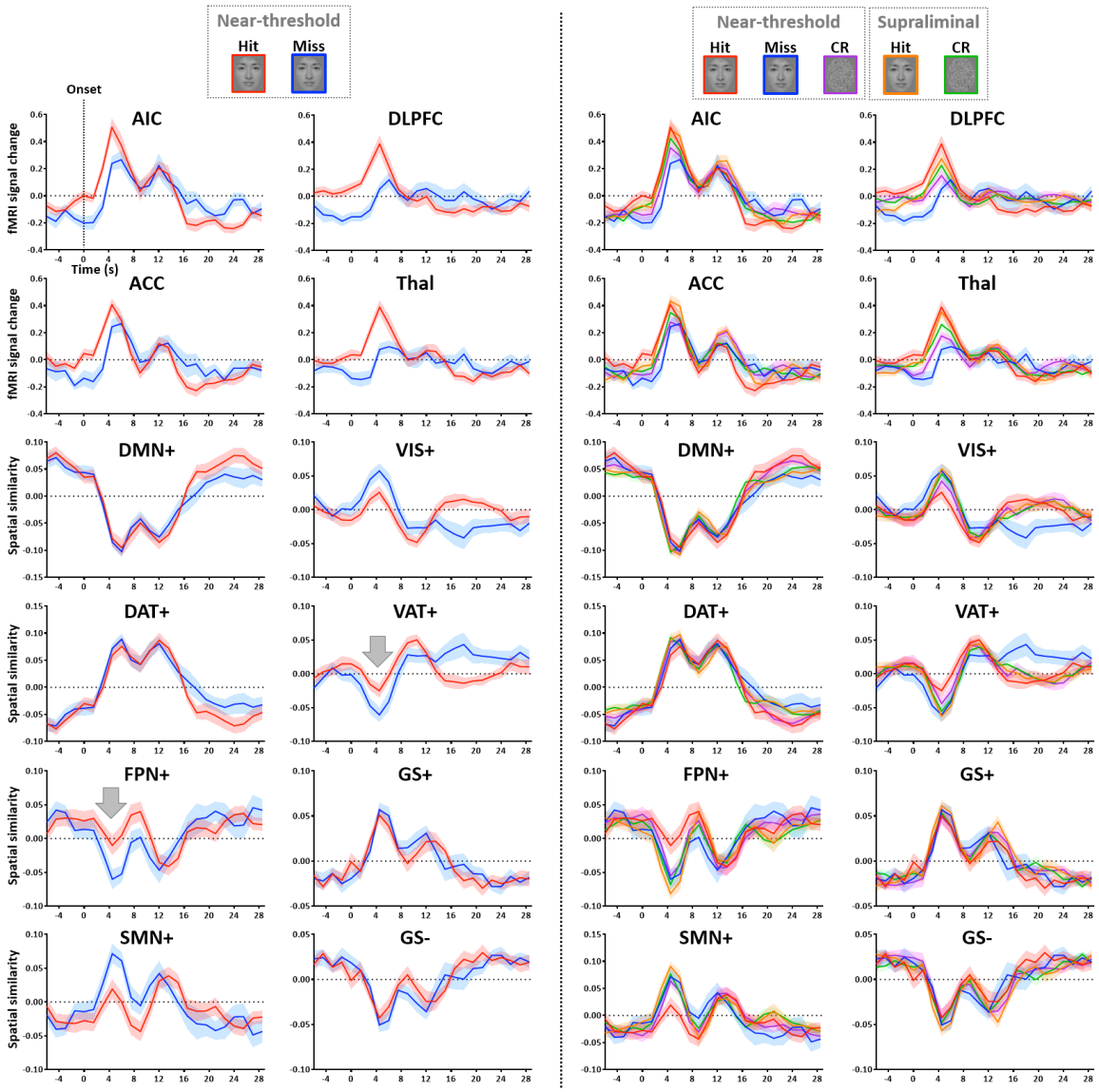

Figure S3. Time course of fMRI signal change (and spatial similarity of CAPs) for supraliminal and near-threshold conditions. Related to Figure 7. Five conditions were compared including near-threshold hit and miss, near-threshold correct rejection (CR), and supraliminal hit and correct rejection. AIC: anterior insular cortex; DLPFC: dorsal lateral prefrontal cortex; ACC: anterior cingulate cortex; Thal: thalamus. The co-activation patterns included the default-mode network (DMN+), dorsal attention network (DAT+), frontoparietal network (FPN+), somatomotor network (SMN+), visual network (VIS+), ventral attention network (VAT+), and global network of activation and deactivation (GN+ and GN-). Shaded areas indicate ±SEM across subjects (n=19).

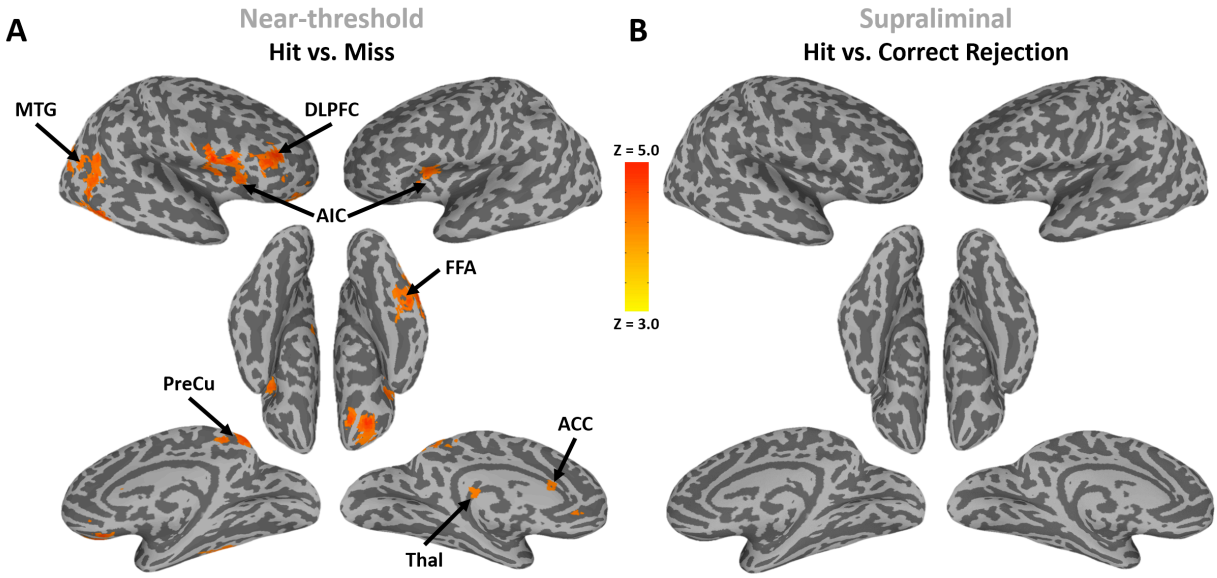

Figure S4. Whole brain contrast at the stimulus onset. Related to Figure 7. Group-level z-maps of fMRI signal intensity are shown for near-threshold hit vs. miss, and supraliminal hit vs. correct rejection (n=19). The z-maps were thresholded at cluster level $\alpha < 0.05$. AIC: anterior insular cortex; DLPFC: dorsal lateral prefrontal cortex; ACC: anterior cingulate cortex; Thal: thalamus; MTG: medial temporal gyrus; PreCu: precuneus; FFA: fusiform face area.

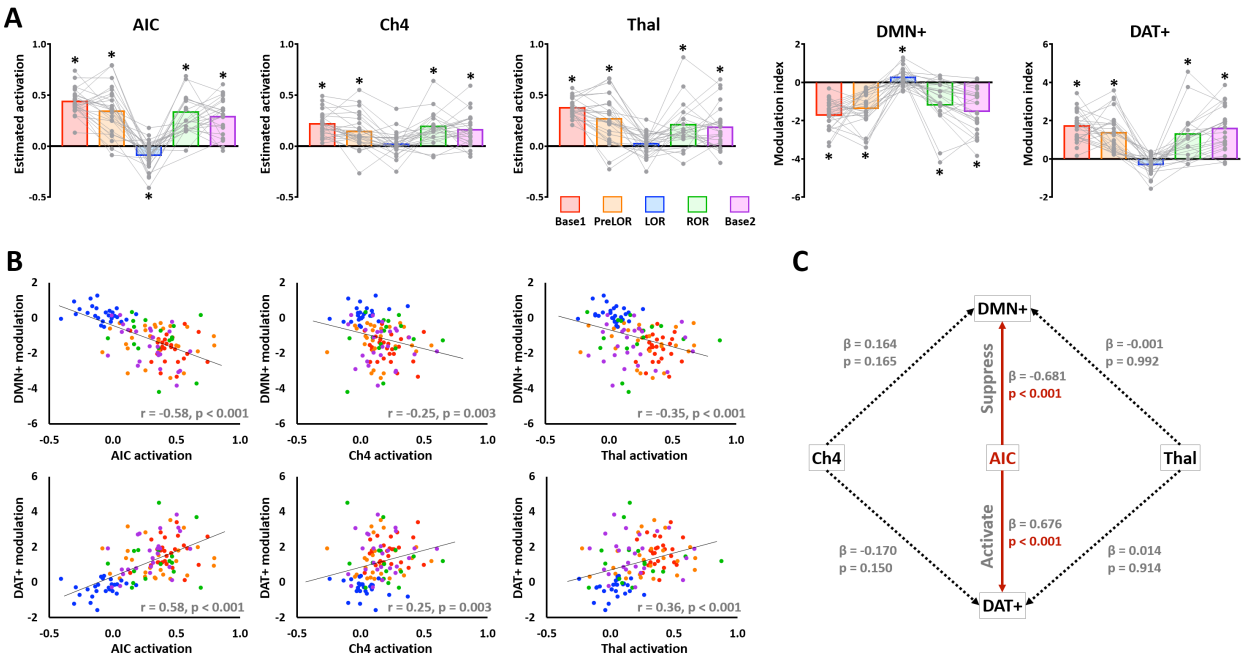

Figure S5. Relationship between AIC, Ch4, Thal and DMN-DAT switch. Related to Figure 6. **(A)** Instruction-evoked activation estimated from general linear model was plotted for AIC, Ch4 and Thal. Modulation indices were plotted for DMN+ and DAT+. Each grey dot represents an individual participant during Base1 (n=26), PreLOR (n=26), LOR (n=26), ROR (n=16), or Base2 (n=25) connected by grey lines across conditions. Bars represent the group averages for each condition. *indicates statistical significance (one sample t-tests against zero) at FDR-corrected alpha <0.05. **(B)** Pearson correlations (n=119) between the regional activation (AIC, Ch4 and Thal) and large-scale network modulation (DMN+ and DAT+). **(C)** Results from multivariate linear regression analysis (n=119) with the estimated activation in the AIC, Ch4 and Thal as independent variables, and the modulation indices in the DMN+ (and DAT+; analyzed separately) as dependent variables. Of the three independent variables tested, only AIC contributes with statistically significance to the DMN-DAT modulation.

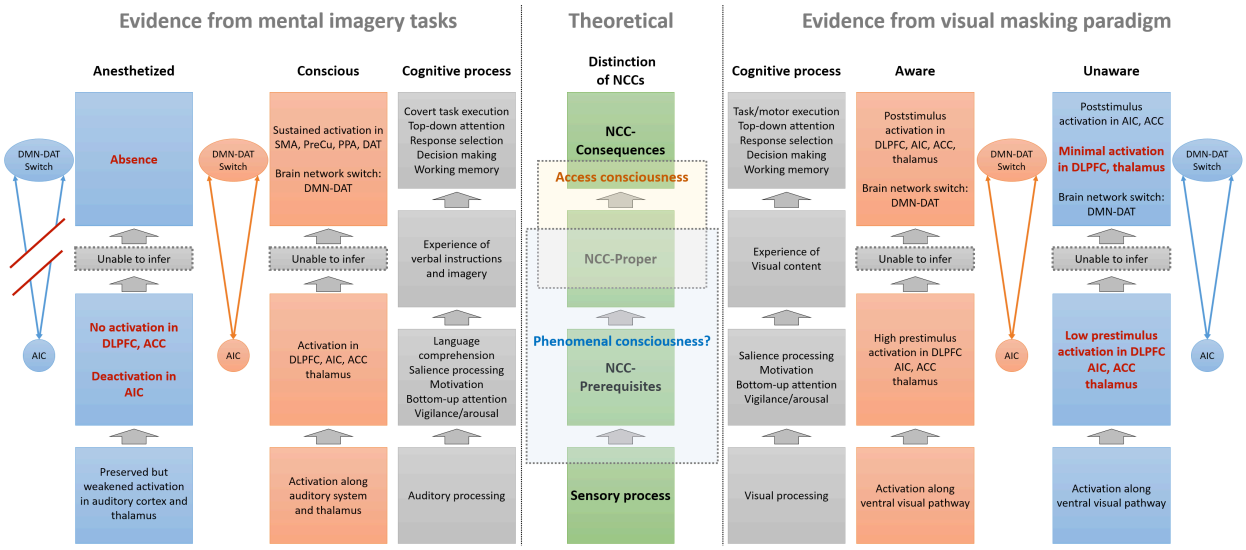

Figure S6. Schematic illustration of the rationale of experimental design and interpretation with respect to the terminology and theoretical aspect of consciousness. Related to Figure 4, Figure 5, Figure 6, and Figure 7. The middle column outlines different neural processes during conscious processing. The neural correlates of consciousness are theoretically dissociated from the prerequisites for and consequences of conscious processing (Aru et al., 2012). The left and right panels summarize the main results from the mental imagery and visual masking tasks. They are aligned to the presumed chains of cognitive processes and theoretical distinctions of NCCs.

Table S1. Summary of regions of interest. Related to Figure 3.

Anatomic structures	Abbreviations	BA	x [R]	y [P]	z [I]	z-value
Right Middle Temporal Gyrus	A1	21	59	-13	-7	7.90
Left Superior Temporal Gyrus	A1	21	-58	-19	2	7.66
Right Middle Frontal Gyrus	DLPFC	10	35	35	20	3.50
Left Middle Frontal Gyrus	DLPFC	10	-34	44	8	3.44
Left Insula	AIC	13	-31	20	2	4.72
Right Insula	AIC	13	32	17	2	4.28
Left Precentral Gyrus	M1	4	-36	-22	51	10.80
Right Medial Frontal Gyrus	MPFC	8	8	56	8	-4.07
Right Cingulate Gyrus	PCC	23	5	-49	26	-3.22
Left Precuneus	PPA	31	-13	-64	23	2.95
Right Posterior Cingulate	PPA	30	23	-58	17	3.07
Right Postcentral Gyrus	PostC	5	20	-43	65	-3.18
Left Postcentral Gyrus	PostC	5	-22	-37	68	-2.98
Left Precuneus	PreCu	7	-7	-70	41	4.77
Right Precuneus	PreCu	7	11	-70	41	4.25
Left Medial Frontal Gyrus	SMA	6	-4	2	50	6.84
Right Middle Occipital Gyrus	Vis	18	41	-82	2	-3.55
Left Inferior Occipital Gyrus	Vis	18	-37	-85	-4	-3.38

BA: Brodmann area; Talairach coordinates are provided for the peak voxel in a given region.